Dyes and Pigments 102 (2014) 241–250

Contents lists available at ScienceDirect

Dyes and Pigments

journal homepage: www.elsevier.com/locate/dyepig

Substituent effects on absorption spectra of pH indicators: An experimental and computational study of sulfonphthaleine dyes

Thierry De Meyer [a,b], Karen Hemelsoet [b], Veronique Van Speybroeck [b,**], Karen De Clerck [a,*]

[a] Department of Textiles, Technologiepark 907, 9052 Zwijnaarde, Belgium
[b] Center for Molecular Modeling, Technologiepark 903, 9052 Zwijnaarde, Belgium

ARTICLE INFO

Article history:
Received 9 September 2013
Received in revised form
29 October 2013
Accepted 30 October 2013
Available online 13 November 2013

Keywords:
Sulfonphthaleine dyes
Halochromism
TD-DFT
UV–Vis spectroscopy
Substituent effects
pK_a

ABSTRACT

Sulfonphthaleine dyes are an important class of pH indicators, finding applications in novel (textile) sensors. In this paper, we present a combined experimental and theoretical study to elucidate the halochromic behaviour of a large set of sulfonphthaleine compounds. Starting from an experimental analysis consisting of UV–Vis spectroscopy, the pH region and the absorption wavelengths related to the colour shift are obtained and pK_a values are derived. The effect of the substituents on the pH region can be traced back to their electron donating/withdrawing properties. Time-Dependent Density Functional Theory (TD-DFT) is able to adequately produce the trend in experimental wavelengths. Proton affinities are used to assess the effect of substituents on the pH region. The combination of theory and experiment is able to give a better understanding of the pH sensitivity; the methodology in this work will be useful in future dye design and is applicable to other dye classes as well.

1. Introduction

Besides their original use as colourants, dyes are increasingly applied in other fields, such as photovoltaic cells, optical switches and light emitting diodes [1,2]. Some dyes show chromic properties, meaning that they change colour depending on an external influence [3]. The most exploited chromic types are thermochromism and photochromism [4,5], but halochromism (pH sensitivity) is also increasingly studied and put into practice [6–12]. Our main interest lies in the possible application of halochromic dyes in pH-responsive polymers, or more precisely intelligent textiles. This is part of a larger research field, namely functionalized polymers [13–16]. It has been shown that pH indicators can be applied on conventional textile materials, thus creating novel sensor materials [17–23]. One of the many applications of such textile sensors is in wound dressings [11]. These textile sensors maintain all advantages of textile materials, meaning they are flexible, applicable on large surfaces and can give a local signal, in particular local discolouration. This colour change is easy to perceive and can be used as a first warning signal. In literature, several examples of sensors based on pH-sensitive dyes can be found [24–31].

A first step towards understanding the interaction of a dye molecule with a textile matrix can be made by studying the molecule solvated in water. We recently elucidated the pH-sensitive behaviour of the azo dye Ethyl Orange [6]. Accurate UV–Vis spectra of the dye in a water environment were simulated using molecular dynamic simulations combined with TD-DFT; which were in good agreement with experiment. The focus of the present paper is to use a similar combined theoretical and experimental approach on a set of sulfonphthaleine dyes. Although this is a small dye class (especially compared to azo dyes), they are widely used as acid–base indicators because they show one or two clearly defined colour transitions as function of pH [32]. Instead of focussing on accurate predictions for one molecule, the scope of this paper is on the detailed examination of a set of dyes based on the same chromophore. It was previously shown in literature that substituents can have large effects on the pH region [12]. This will allow us to gain more insight into qualitative trends and to understand the effect of substituents on the halochromic behaviour. Based hereon,

* Corresponding author. Department of Textiles, Ghent University, Technologiepark 907, B-9052 Zwijnaarde, Belgium. Tel.: +32 9 264 57 35; fax: +32 9 264 58.
** Corresponding author. Center for Molecular Modeling, Ghent University, Technologiepark 903, 9052 Zwijnaarde, Belgium. Tel.: +32 9 264 65 61.
E-mail addresses: thierry.demeyer@ugent.be (T. De Meyer), karen.hemelsoet@ugent.be (K. Hemelsoet), veronique.vanspeybroeck@ugent.be (V. Van Speybroeck), karen.declerck@ugent.be (K. De Clerck).

0143-7208/$ – see front matter © 2013 Elsevier Ltd. All rights reserved.
http://dx.doi.org/10.1016/j.dyepig.2013.10.048

certain predictions will be possible for hypothetical dyes with the same chromophore and for existing dyes in another environment (for instance a textile matrix). Eventually studies of these systems should allow for future design of tailor-made dyes for a specific application [33].

The basic structure of sulfonphthaleine dyes is given in Fig. 1; the substituents of the studied molecules are also listed [1,34]. The dye set in this work contains 10 molecules and covers most commercially available sulfonphthaleine compounds. These products have numerous applications [35–41], often in biological and medical fields [42–53]. Sulfonphthaleine dyes are not only sensitive to pH, but are also used in sensor applications for detecting pesticides, CO_2 and ammonia [54–56]. The development of new glassy carbon electrodes also deserves mention [57–60]. Other interesting studies include the hyperpolarizabilities of these dyes and also the possibility to serve as starting point for the development of new dyes [61,62]. Phenol Red (**1**) has no substituents and is therefore ideally suited to form the start of our discussion.

In this work a combined theoretical and experimental approach is used to unravel the behaviour of sulfonphthaleine dyes in aqueous solution. Molecular simulations provide insight on a molecular scale and can help to understand the cause of a colour change. All theoretical calculations in this work are performed using Density Functional Theory (DFT). Excited states are calculated starting from an optimized ground state geometry, followed by a vertical excitation energy, the latter within the Time-Dependent variant of DFT (TD-DFT) [63–65]. TD-DFT is widely used and often provides accurate results [66]. Although TD-DFT is formally exact, practical implementation leads to approximations due to the nature of the exchange-correlation (xc) functional and the usually applied adiabatic approach [67]. In this light, an important issue is a charge-transfer (CT) [68]. To tackle this problem, several long-range corrected functionals have been developed, for example the Coloumb Attenuated version of B3LYP (CAM-B3LYP) [69–71].

Several groups have studied dye molecules with TD-DFT [72–77] and extensive benchmark studies have been performed by Jacquemin et al. [66,78–84]. They have shown that more conventional hybrid functionals, such as B3LYP, perform quite well in general, but long-range corrected functionals provide a beneficial effect for dyes exhibiting CT character. A diagnostic tool has been developed by Peach et al. to determine the magnitude of the CT and thus the likeliness of artifacts [85–87]. The same authors have also pointed out the improvement compared to experiment of the Tamm-Dancoff approximation (TDA) when there is a triplet instability, caused by the exact exchange used in hybrid functionals [88–90]. Both errors seem to cause an underestimation of the excitation energy compared to experiment.

The goal of this paper is threefold: (i) we want to gain a better understanding of the pH-sensitive behaviour of sulfonphthaleine dyes and (ii) the influence of the substituents hereupon; (iii) we also want to achieve a theoretical model in which simple calculations can be used to predict the pH region of the colour change. The latter is useful for future dye design and can help further research where the environment is taken into account. Because of the direct link to the colour of the species, the experimental part will mainly consist of characterization by UV–Vis spectroscopy in different pH environments. First the observations for Phenol Red will be discussed and second the substituent effects will be studied. Thorough understanding of the observed effects at the molecular level is achieved by molecular modelling. The present work covers the behaviour of dyes in solution. It forms the basis of future research when the interaction between dye molecules and a polymer/textile matrix is considered.

2. Materials and methods

All dye molecules were supplied by Sigma–Aldrich, together with hydrochloric acid (1 mol/1) and sodium hydroxide (50 m%) for pH regulation. Measurement of the pH values were executed with a Hamilton glass electrode and a SympHony pH meter. Experimental UV–Vis spectra of a 10 mg/l solution were measured on the Lambda 900 spectrophotometer from Perkin–Elmer in the interval 200–800 nm (with a resolution of 1 nm). The transmission measurements in solution are recalculated to absorbance. pK_a values are calculated from absorbance spectra using following formula [91,92]:

$$pK_a = pH - \log\left(\frac{A_z - A_a}{A_b - A_z}\right) \quad (1)$$

in which A_z is the absorbance obtained at a defined pH and A_a and A_b are the absorbance of the acid and base form respectively. In this work, it was chosen to calculate the pK_a for each measured pH value and subsequently take the average.

3. Theory and calculations

All calculations were carried out in Gaussian09 [93] using Density Functional Theory (DFT), as this method is both

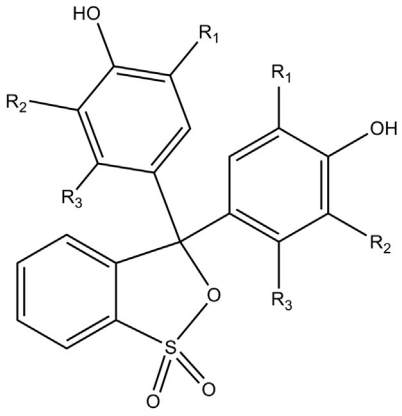

	R_1	R_2	R_3
(**1**) Phenol Red	H	H	H
(**2**) Cresol Red	CH_3	H	H
(**3**) m-Cresol Purple	H	H	CH_3
(**4**) Xylenol Blue	CH_3	H	CH_3
(**5**) Thymol Blue	*i*-Pr	H	CH_3
(**6**) Chlorophenol Red	Cl	H	H
(**7**) Bromophenol Blue	Br	Br	H
(**8**) Bromocresol Purple	Br	CH_3	H
(**9**) Bromocresol Green	Br	Br	CH_3
(**10**) Bromothymol Blue	*i*-Pr	Br	CH_3

Fig. 1. Basis structure of sulfonphthaleine dyes and substituents of the studied compounds.

computationally efficient and sufficiently accurate for examining large dye molecules. Geometries were optimized using the B3LYP electronic structure method in combination with a 6-31+G(d,p) basis set [94,95]. The B3LYP functional combined with a Pople basis set of double-zeta quality for the valence orbitals was more specifically shown to produce geometries [96] and corresponding frequencies in good agreement with experimental data of other dyes [97–99]. Curtiss et al. showed that B3LYP generates geometries comparable to those of second order Møller–Plesset perturbation theory (MP2) [100,101]. Frequency calculations were performed at the same level of theory as the geometry optimization to obtain zero-point vibrational energy and Gibbs free energy corrections [102]. B3LYP is a hybrid functional, using 20% exact exchange (20% Hartree–Fock, HF). Besides B3LYP, other functionals were tested in this work with varying amounts of exact exchange: PBE (pure GGA, no exact exchange) [103,104]; M06-2X (meta hybrid functional containing 54% HF exchange) [105] and CAM-B3LYP (hybrid with variable amount of HF exchange, between 19% and 65%) [71].

Conformational analysis and frequency calculations were performed to find the absolute minimum for each compound. All calculations were performed with inclusion of implicit solvation, which is modelled using the standard self-consistent reaction field in Gaussian09; namely the Integral Equation Formalism Polarizable Continuum Model (IEF-PCM) [106–108]. UV–Vis spectra were calculated with TD-DFT using 30 excited states. These computations involve optimized ground state geometries and hence vertical excitation energies are obtained. To evaluate the influence of the DFT functional on the calculated UV–Vis spectra, PBE, B3LYP, M06-2X and CAM-B3LYP were tested, using geometries optimized with the functional used for the TD-DFT calculation. The computational details concerning the molecular dynamic simulation can be found in Section S1 of the Supporting Information (SI).

4. Results and discussion

4.1. Experimental study: pH-sensitive mechanism and substituent effects

4.1.1. Phenol Red

Looking at the basic structure of the sulfonphthaleine dyes (Fig. 1), it can easily be understood that these molecules will behave as acids in water. When solvated, deprotonation will allow for a rearrangement of the internal bonds (Scheme 1 illustrates the behaviour for **1**). The driving force behind this deprotonation is twofold: the internal rearrangement results in a larger conjugated system and a SO_3^- group is formed ($\mathbf{1}_a$). The latter allows for a high interaction with the surrounding water molecules and is thus energetically favourable. The deprotonation was experimentally verified by a drop in pH upon solvation of **1**.

The internal rearrangement can be confirmed by molecular modelling. In Fig. 2, the gas phase structures of $\mathbf{1}_a$ are given: the compound on the left-hand side has the bond between the oxygen and central carbon atom, while the structure at the right-hand side has a free SO_3^- group. It was seen in a molecular dynamic simulation with explicit solvent that the bond spontaneously breaks, indicating a very low barrier (see Section S1 of the SI for Computational Details). The internal rearrangement results in a Gibb's free energy drop of 71 kJ/mol. The latter form is also only stable when an implicit solvation model is taken into account, which is why all calculations in this work are performed with PCM.

Phenol Red (**1**) is the simplest (unsubstituted) structure of the class of sulfonphthaleine dyes and we will first focus on this molecule. The most important analytical tool when studying the colour change is the UV–Vis spectrum of **1** in aqueous solution with

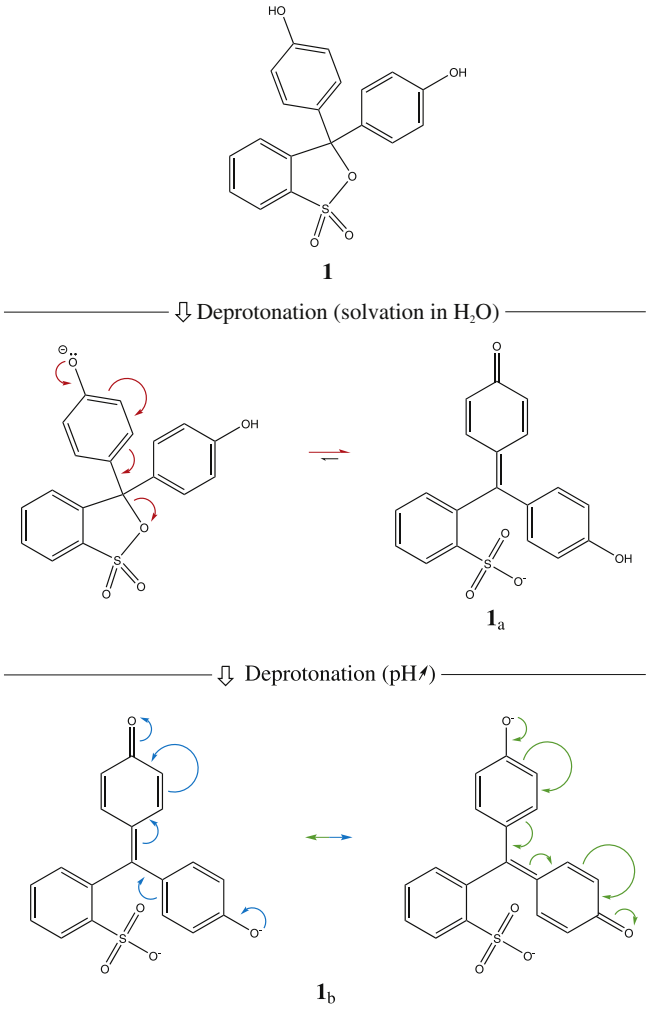

Scheme 1. In aqueous solution, **1** acts as an acid and the molecule looses a proton, which results in a rearrangement of the internal bonds ($\mathbf{1}_a$). When going to more alkaline media (above pH 6), a deprotonation results in the resonance stabilized form $\mathbf{1}_b$.

changing pH. The absorption spectra of **1** and the intensity of main absorption peaks are shown in Fig. 3(a) and (b), respectively. The form obtained when solvating the molecule ($\mathbf{1}_a$) is stable between pH 2 and pH 6 and has its absorption maximum (λ_{max}) at 433 nm (yellow). Going to more alkalic media (between pH 6 and 9), **1** exhibits a colour change. This indicates another deprotonation, as shown in Scheme 1. This scheme was also proposed in literature and is confirmed here (vide infra) [32,109]. **1** also shows a colour change in acidic media; the full-range spectrum is given in Section S2 of the SI. The colour change around neutral pH is of most interest for the application as wound bandages and hence will further be explored (Fig. 3(a)).

The pH region of the colour change of **1** is thus pH 6–9, which can be seen more clearly from Fig. 3(b). Using Formula (1), the pK_a of **1** can be calculated as 8.0. Alternatively, the pK_a can also be estimated from the crossing point in Fig. 3(b). The colour changes from yellow to red, which corresponds with a shift of λ_{max} from 433 nm to 559 nm. There is an isosbestic point at 480 nm, confirming a colour change between two clearly defined structures. It is also worth noting that the structure in a basic environment ($\mathbf{1}_b$) is stabilized by resonance (see Scheme 1). This is further verified by molecular modelling in Section S3 of the SI.

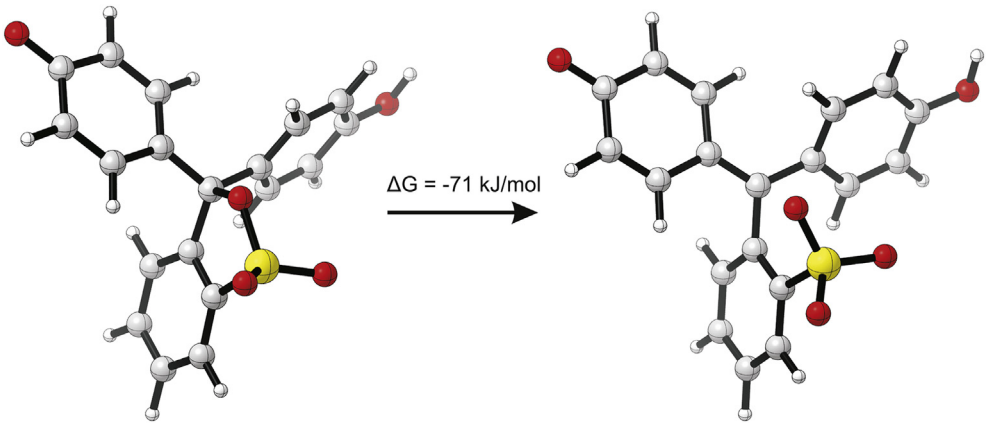

Fig. 2. Rearrangement of the internal bonds as calculated at the B3LYP/6-31+G(d,p) level of theory (with inclusion of implicit solvent, IEF-PCM). The drop in Gibb's free energy clearly illustrates that the right-hand form ($\mathbf{1}_a$) is more stable.

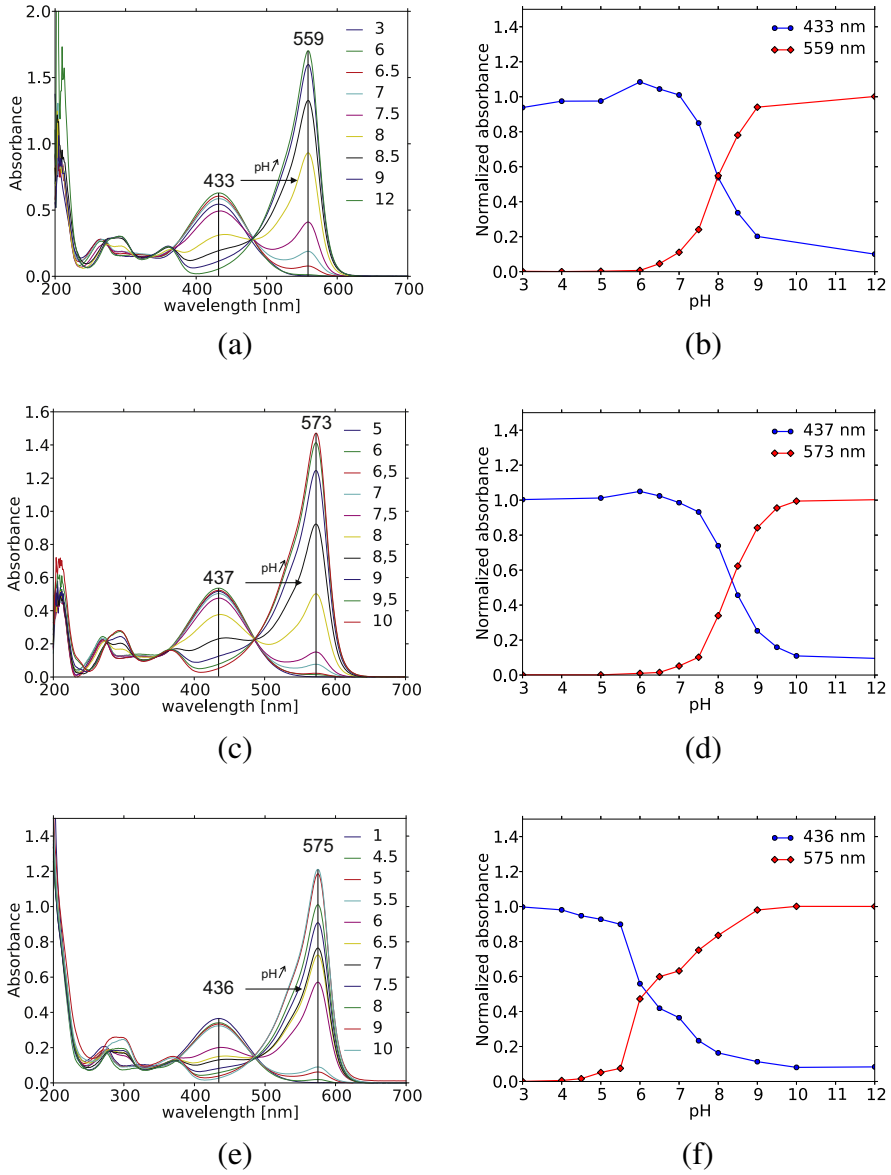

Fig. 3. UV–Vis spectrum of **1**, **2** and **6** in solution (a, c, e respectively) and normalized intensity of the main absorption peaks (λ_{max}) of **1**, **2** and **6** (b, d, f respectively), with altering pH.

4.1.2. Substituent effects

The effect of substituents on the reference structure **1** on the pH-sensitive properties will now be discussed. This includes a shift of the pK_a and the influence on λ_{max}, the so-called auxochromic effect. All data concerning the halochromic properties of the dye set (pH region, corresponding wavelengths λ_{max} and pK_a values) are included in Table 1 [32,110].

The molecules of the test set (Fig. 1) can be divided into three types: those with electron donating substituents (**2**–**5**); with electron withdrawing substituents (**6, 7**) and those with both electron donating and withdrawing groups (**8**–**10**). The UV–Vis spectra of dyes **2** and **6** are included in Fig. 3 as examples of dyes with electron donating and electron withdrawing substituents, respectively. UV–Vis spectra of all compounds are given in Section S2 of the SI.

Before going into detail, some general observations of Table 1 can be made. There is a clear influence of the substituents: electron donating groups will cause the pH region to shift to higher pH values (higher pK_a values), while electron withdrawing substituents have the opposite effect. While the auxochromic effect (influence on λ_{max}) is very small for the components $\mathbf{x}_a$, there is an influence on the colour of $\mathbf{x}_b$. In the latter case, a general rule is the more/larger the substituents, the higher λ_{max} will be.

Cresol Red (**2**) has two methyl substituents, which are electron donating. Hence, compared to **1**, there will be a slightly larger negative charge in the conjugated system. The bond between the proton and oxygen of the hydroxyl group will be stronger and thus deprotonation will be more difficult. This is reflected experimentally with the observation that a slightly more alkaline medium is needed to allow for deprotonation and therefore the colour shift is between pH 7.0 and 9.5 instead of pH 6.5 and 9.0 as for **1** (see also Fig. 3(d)). m-Cresol Purple (**3**) also has two methyl groups and the effects on the pH region are similar. Xylenol Blue (**4**) has four methyl substituents and thus the electron donating effect is larger. The colour change here is shifted to even higher pH values, pH 8.5 to 10.0. The *i*-Pr group in Thymol Blue (**5**) has apparently almost the same effect as a methyl group, while a slightly larger electron donating effect was expected. The substituents only seem to effect the absorption wavelengths of $\mathbf{x}_b$, in which a clear trend is also visible. The two methyl groups in **2** and **3** give rise to a slightly higher λ_{max} than that of **1**. Four methyl groups in **4** and two methyl- and two *i*-Pr groups in **5** again give rise to longer λ_{max} wavelengths.

Electron withdrawing substituents have exactly the opposite effect. The chlorine substituents in Chlorophenol Red (**6**) have a high electronegativity and thus have an electron withdrawing effect. This causes the pH shift to drop from 6.5–9.0 (for **1**) to 5.0–8.0. Even though bromine has a smaller electronegativity, the four substituents in Bromophenol blue (**7**) have a large effect and cause the pH region to drop to 2.5–5.0. In Bromocresol Purple (**8**), the electron withdrawing effect of bromine is countered by the electron donating methyl group; the netto electron withdrawing effect is thus rather small for this molecule. Again, the effects are similar for all structures with electron withdrawing substituents (**6**–**10**).

The observations made in this paragraph already indicate that the facility for deprotonation strongly correlates with the pH region (and thus the pK_a). This will be further examined using proton affinities in Section 4.2.2.

Table 1
pH region of the colour change, pK_a value and corresponding absorption wavelengths (nm and eV between parenthesis) of all compounds **x** shown in Fig. 1 (measured in water). These values are compared to calculated vertical absorption energies E_{vert}.

x	pH region	pK_a	$\lambda_{max}(\mathbf{x}_a)$	$\lambda_{max}(\mathbf{x}_b)$	$E_{vert}(\mathbf{x}_a)$	$E_{vert}(\mathbf{x}_b)$
1	6.5–9.0	8.0	433 (2.86)	559 (2.22)	421 (2.94)	485 (2.56)
2	7.0–9.5	8.3	437 (2.84)	573 (2.16)	428 (2.90)	496 (2.50)
3	7.0–9.5	8.5	435 (2.85)	578 (2.15)	435 (2.85)	510 (2.43)
4	8.0–10.0	9.1	437 (2.84)	594 (2.09)	442 (2.80)	522 (2.37)
5	8.0–10.0	8.9	435 (2.85)	596 (2.09)	442 (2.81)	524 (2.36)
6	5.0–8.0	6.7	436 (2.84)	575 (2.16)	426 (2.91)	492 (2.52)
7	2.5–5.0	4.1	436 (2.84)	591 (2.10)	440 (2.82)	508 (2.44)
8	5.0–7.5	6.3	432 (2.87)	589 (2.11)	423 (2.93)	506 (2.45)
9	3.5–5.5	4.8	443 (2.80)	616 (2.01)	463 (2.68)	530 (2.34)
10	6.5–8.5	7.4	435 (2.85)	617 (2.01)	461 (2.69)	548 (2.26)

4.2. Ab initio simulations

4.2.1. Level of theory assessment on Phenol Red

A Level Of Theory (LOT) study is performed on structure **1** to guarantee the reliability of the theoretical data. Herein several computational methods are compared to choose one most suited for this application. All optimized structures are included in Section S4 of the SI. For reference, both singlet and triplet states were calculated, but the latter proved to be on average 115 kJ/mol higher in Gibbs free energy and are therefore omitted from the discussion. It is noted here that these molecules have multiple local minima with relatively large energy differences. A thorough conformational analysis was thus performed by systematically scanning the local minima in terms of the various dihedral angles.

As already mentioned in the introduction, the choice of exchange-correlation functional can have a strong influence on the results. Therefore, the following functionals were chosen because of their different amount of exact exchange (Hartree–Fock, HF): PBE, B3LYP, M06-2X and CAM-B3LYP. In Table 2 the calculated vertical excitation energies (E) of $\mathbf{1}_a$ and $\mathbf{1}_b$ are compared to experimental λ_{max} values.

An increasing amount of exact exchange results in a larger discrepancy with experiment, which might point toward a triplet instability (see Introduction). However, Peach et al. previously reported that an increase in HF exchange usually leads to a decrease in excitation energy [89,90]. This is clearly not the case and hence TDA is not expected to improve the results. For reference, stability values and TDA results are given in Section S5 of the SI. Overall, the agreement with experiment is rather good in the case of $\mathbf{1}_a$ for PBE and B3LYP, whereas a large difference is found for $\mathbf{1}_b$.

It is noted here that the physical process behind an experimental value is not always well defined, which must be kept in mind when comparing experimental and theoretical results. In addition to vertical excitations as used here, one can also calculate adiabatic values [111]. This means that the energy difference between the optimized ground state and optimized excited state is calculated; which is the energy difference between the two minima as depicted in Fig. 4. For the vertical excitation on the other hand (as used in this work), only the optimized ground state geometry is used.

Adiabatic values are especially interesting in the light of cyanine dyes. These molecules show a delocalized charge and are in that aspect similar to $\mathbf{1}_b$ (see also Section S3 of the SI). These delocalized charges were until recently considered problematic for TD-DFT

Table 2
Computed absorption maxima (in nm, eV between parenthesis) of $\mathbf{1}_a$ and $\mathbf{1}_b$ (6-31+G(d,p) basis set), compared to experimental data.

nm	% HF exchange	$\mathbf{1}_a$	$\mathbf{1}_b$
PBE	0	467 (2.66)	520 (2.39)
B3LYP	20	421 (2.95)	485 (2.56)
M06-2X	54	374 (3.32)	473 (2.62)
CAM-B3LYP	19–65	368 (3.37)	465 (2.67)
Exp (λ_{max})		433 (2.86)	559 (2.22)

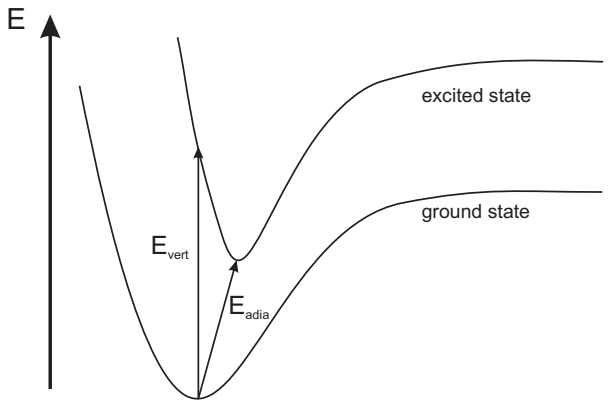

Fig. 4. Schematic representation of vertical and adiabatic excitation.

[112,113]. Send et al. however indicated that the nature of the excitation might be essentially non-vertical and that TD-DFT is not the cause of the discrepancy [114]. This would mean that the 'true' excitation that occurs in the absorption experiment is not completely vertical and thus lightly shifted towards the adiabatic excitation. This also means that vertical excitation energies will generally be larger than the observed experimental energies, as is the case here. Cyanine dyes were further studied by Jacquemin and coworkers. In a recent study they compared experimental adiabatic and theoretical adiabatic values, finding a much better agreement [115,116]. One must keep in mind however that these experimental adiabatic values are different from the λ_{max} values obtained by absorbance spectra. The latter are of course our main interest because they determine the colour of the species. Because only absorption data are at hand, qualitative comparisons with experiment can still be made in the vertical approximation as will be shown further on.

Of all functionals tested, PBE and B3LYP perform best compared to experiment. However, PBE did show some so-called dark states (the values given in Table 2 are the lowest in energy with a minimal oscillator strength of 0.1), which were absent in the case of B3LYP. Compared to PBE, B3LYP has proven itself to be a more than adequate method for calculating geometries and energies, which makes it a more promising method for future research when the environment will be taken into account. As shown later on, B3LYP is able to qualitatively predict the trend in the excitation energies. Therefore, further calculations in this work will thus be performed using B3LYP; which was also the method of choice in our previous work [6].

Table 2 shows that the B3LYP method is good for reproducing experimental values at low pH. The discrepancy, observed at high pH, is not easily solved because of the physical nature of the excitation. It will be shown in the next paragraph that the selected method, however, succeeds at elucidating the qualitative experimental trend in terms of the substituents.

4.2.2. Theoretical study of the dye set

For each structure, the vertical excitation energy is calculated for both the acidic ($E_{vert}(\mathbf{x}_a)$) and basic ($E_{vert}(\mathbf{x}_b)$) form and all data is listed in Table 1. The remarks made for structure **1** are valid for all structures in our test set: λ_{max} of the acidic form $\mathbf{x}_a$ is always well reproduced, with an absolute mean deviation of only 10.2 nm (0.07 eV). The overestimation of λ_{max} for the basic form $\mathbf{x}_b$ is much larger but quite constant (on average 76.7 nm, 0.31 eV). To better illustrate that the trend is maintained, all structures are given in decreasing order of λ_{max} of the basic form $\mathbf{x}_b$ in Section S6 of the SI, showing that the experimental order is almost equal to the theoretical order. For reference, the reactivity of all involved molecules has been studied (see Section S3 of the SI). The $\mathbf{x}_b$ compounds are found to be more reactive than $\mathbf{x}_a$, however little influence of the substituents is seen.

The effect of substituents on the pH range of the colour change can be understood using proton affinities (PAs) of the implicitly solvated compounds. The following discussion is easily expanded to any other pH-dependent (de)protonation. Using **1** as example, consider the reaction when a proton is added to the molecule:

$$\mathbf{1}_b + \mathrm{H}^+ \rightarrow \mathbf{1}_a \tag{2}$$

The equilibrium constant can be written as:

$$K_{\mathbf{1}} = A_{\mathbf{1}} \mathrm{e}^{-\Delta G_{\mathbf{1}}/RT} \tag{3}$$

with $\Delta G_{\mathbf{1}} = G_{\mathbf{1}_a} - G_{\mathbf{1}_b} - G_{\mathrm{H}_1^+}$; which can also be written in function of the PA: $\Delta G_{\mathbf{1}} = PA_{\mathbf{1}} - G_{\mathrm{H}_1^+}$.

A PA can thus be considered as the drop in Gibbs free energy when adding a proton. When comparing the PAs of two different compounds, the molecule with the lowest PA (more negative) will be able to stabilize the proton more than the other molecule. This can also be interpreted that protonation will be easier. Note that PAs are sometimes also defined in terms of energy or enthalpy instead of Gibbs free energy as used here.

Another way of writing the equilibrium constant is based on the activities of the different compounds:

$$K_1 = \frac{\mathrm{a}_{\mathbf{1}_a}}{\mathrm{a}_{\mathbf{1}_b}\mathrm{a}_{\mathrm{H}_1^+}} \tag{4}$$

Note that the equilibrium constant depends on the environment, in this case the pH. The pH that is assumed here, is the pK_a. When $\mathrm{pH} = \mathrm{pK}_a$, both components have the same concentration ($\mathrm{a}_{\mathbf{1}_a} = \mathrm{a}_{\mathbf{1}_b}$) which also means the middle of the colour transition. In the case of **1**, pH = 8.0 (see Table 1 and Fig. 3(b)). The previous rationale also applies for another compound, for example **2**, but do note this is at a different pH (more specifically pH 8.3 for **2**). The ratio of both equilibrium constants can then be written as (5) and simplified to (6).

$$\frac{K_{\mathbf{1}}}{K_{\mathbf{2}}} = \frac{A_{\mathbf{1}}\mathrm{e}^{-\frac{\Delta G_{\mathbf{1}}}{RT}}}{A_{\mathbf{2}}\mathrm{e}^{-\frac{\Delta G_{\mathbf{2}}}{RT}}} = \frac{\frac{\mathrm{a}_{\mathbf{1}_a}}{\mathrm{a}_{\mathbf{1}_b}\mathrm{a}_{\mathrm{H}_1^+}}}{\frac{\mathrm{a}_{\mathbf{2}_a}}{\mathrm{a}_{\mathbf{2}_b}\mathrm{a}_{\mathrm{H}_2^+}}} \tag{5}$$

$$\frac{A_{\mathbf{1}}}{A_{\mathbf{2}}}\mathrm{e}^{\frac{-(\Delta G_{\mathbf{1}} - \Delta G_{\mathbf{2}})}{RT}} = \frac{\mathrm{a}_{\mathrm{H}_2^+}}{\mathrm{a}_{\mathrm{H}_1^+}} \tag{6}$$

Taking the logarithm base 10 on both sides of (6) results in:

$$\ln\left(\frac{A_{\mathbf{1}}}{A_{\mathbf{2}}}\right) + \frac{-\Delta G_{\mathbf{1}} + \Delta G_{\mathbf{2}}}{RT} = \ln(10)\left[\log\left(\mathrm{a}_{\mathrm{H}_2^+}\right) - \log\left(\mathrm{a}_{\mathrm{H}_1^+}\right)\right] \tag{7}$$

Using PAs and the definition of pH, this can be written as:

$$\ln\left(\frac{A_{\mathbf{1}}}{A_{\mathbf{2}}}\right) + \frac{-\mathrm{PA}_{\mathbf{1}} + \mathrm{PA}_{\mathbf{2}} + G_{\mathrm{H}_1^+} - G_{\mathrm{H}_2^+}}{RT} = \ln(10)(\mathrm{pH}_{\mathbf{1}} - \mathrm{pH}_{\mathbf{2}}) \tag{8}$$

As a final assumption, we set $G_{\mathrm{H}_1^+} - G_{\mathrm{H}_2^+}$ to be constant, which allows us to use PAs instead of ΔG values. Defining $\Delta\mathrm{PA} = \mathrm{PA}_{\mathbf{2}} - \mathrm{PA}_{\mathbf{1}}$ and $\Delta\mathrm{pH} = \mathrm{pH}_{\mathbf{2}} - \mathrm{pH}_{\mathbf{1}}$ and knowing that $\ln(A_{\mathbf{1}}/A_{\mathbf{2}})$ is also constant allows us to finally write (8) as:

$$\Delta\mathrm{PA} = -RT\ln(10)\Delta\mathrm{pH} + C = -RT\ln(10)\Delta\mathrm{pK}_a + C \tag{9}$$

The linear behaviour is quite easy to understand: the more stabilized the molecule is upon protonation; the lower the pH

region will be. This correlation is illustrated in Fig. 5; the PA (relative to **1**, absolute values can be found in Section S7 of the SI) is plotted as function of the pH range of the colour change for each dye studied here. At first glance, the linear behaviour is quite obvious. The regression constant of the linear behaviour is 98%.

It is noted here that the slope of the linear regression is not equal to $-RT\ln(10)$, in contrary to (9). This is because $G_{H_1^+} - G_{H_2^+}$ was set to be constant, while G_{H^+} is in fact dependent on the pH and thus linked to the calculated PA. Several literature studies concern the calculation of pK_a values [117–121]. Most studies use high-accuracy methods (such as CBS-QB3); the DFT results obtained here are a more economical solution when computer time is concerned. Some of these studies use experimental values for G_{H^+}, but a fixed value would result in the same deviation [122,123]. One could use a linear model for G_{H^+} in function of calculated PAs, but the transferability of these results would be questionable. In any case, these actions would not improve our understanding of the experimental trend and the qualitative trend found here was the goal of this discussion.

The linear behaviour can be used to predict the pH region of hypothetical sulfonphthaleine dyes. A simple PA calculation is sufficient to have an idea in what range the colour transition will occur. The linear dependence of PA and the pH region is of course not limited to this dye set; it holds for any pH-sensitive system. Combined with TD-DFT calculations, one can predict both the pH region and the corresponding colour shift of hypothetical dyes. This knowledge can also be applied when studying dyes in different environments. It would be interesting to see how the PA changes when a dye is put into a textile matrix for instance and how this relates to a change in pH region. This will be the subject of future research.

4.3. Validation for sulphamphtaleine dyes

Sulfonphthaleine dyes have been modified by Bhuchar and Agrawal to sulphamphthaleine dyes [62]. More specifically, Phenol Red (**1**) and Cresol Red (**2**) were modified by substituting an oxygen of the SO_3^- group by NH^-, resulting in a SO_2NH^- group. The two final structures, labelled **11** and **12**, are shown in Fig. 6.

The proposed methodology is now applied to these two new structures and compared with the experimental findings of Bhuchar and Agrawal. All data is given in Table 3. The pK_a values of **11** and **12** were derived by calculating their respective PAs and then applying the linear regression found for Sulfonphthaleine dyes (see Fig. 5). The resulting pK_a values are quite close to the experimental ones.

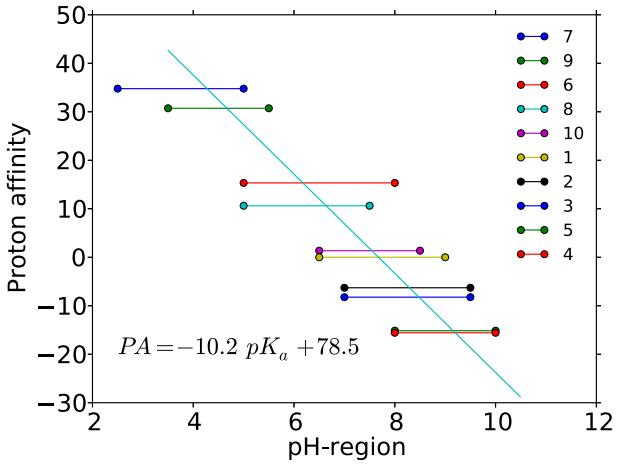

Fig. 5. The theoretical PA (kJ/mol, relative to **1**) as function of the pH region of the colour change clearly illustrates the linear dependence of both quantities.

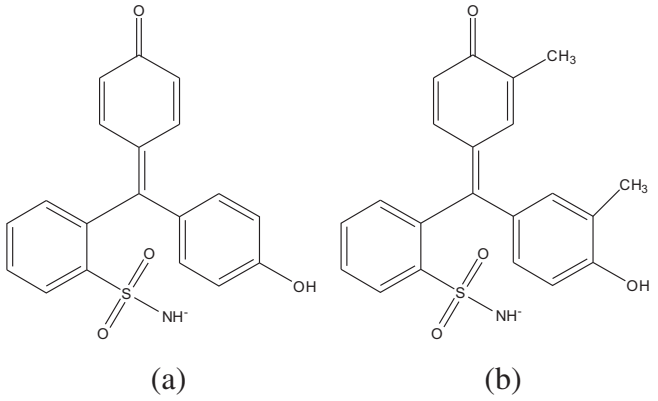

Fig. 6. Schematic representation of (a) phenolsulphamphthalein, **11**, and (b) cresolsulphamphthalein, **12**, as synthesized by Bhuchar et al [62].

The calculated vertical absorption wavelenghts are in agreement with the results found for the sulfonphthaleine dyes. For $\mathbf{11}_a$ and $\mathbf{12}_a$ the results are close to experimental values, while the wavelengths for $\mathbf{11}_b$ and $\mathbf{12}_b$ are again underestimated. It is noted that this underestimation is almost the same as the average 76.6 nm found for sulfonphthaleine dyes. Keeping this in mind, we can thus say that the model is able to predict the pH-region (pK_a) and colour of both sulphamphtaleine dyes.

5. Conclusions

In this work, we have studied 10 sulfonphthaleine dyes using both experimental and theoretical techniques. The combination of both disciplines has helped to unravel the molecular structures involved in the colour change, rationalizing the colour changing mechanism found in literature. Experimental UV–Vis spectra were measured to analyse the halochromic behaviour of each dye and to substract the two important parameters: the pH region of the colour change (with corresponding pK_a value) and the absorption wavelengths λ_{max}. Specifically the effect of electron donating and withdrawing groups was studied. Both experimental parameters were elucidated using molecular modelling. Vertical absorption energies calculated with TD-DFT showed an adequate agreement with experimental data. The pH region of the colour change could be explained using Proton Affinities (PAs) and a linear dependence was deducted. The combination of TD-DFT calculations and PAs is able to fully interpret experimental data and can thus be used to predict the colour shift and pH region of hypothetical sulfonphthaleine dyes. This was illustrated for modified sulfonphthaline dyes, in particular sulphamphthaleine dyes. The methodology proposed in this paper can be generalized to other dye classes and is promising for future dye-design.

Table 3
Calculated pK_as and absorption wavelengths for sulphamphthaleine dyes (**11** and **12**), compared to experimental data from Bhuchar and Agrawal [62]. Wavelengths are in nm and eV between brackets.

pK_a				
	11		**12**	
Exp	7.96		8.32	
Theo	7.75		8.33	
λ_{max}				
	$\mathbf{11}_a$	$\mathbf{11}_b$	$\mathbf{12}_a$	$\mathbf{12}_b$
Exp	423 (2.93)	481 (2.58)	426 (2.91)	494 (2.51)
Theo	440 (2.82)	560 (2.21)	440 (2.82)	575 (2.16)

Acknowledgements

The Fund for Scientific Research Flanders (FWO) and the Research Board of Ghent University (BOF) are acknowledged for their financial support. Computational and experimental resources and services used in this work were provided by Ghent University. Support is acknowledged by the Interuniversity Attraction Poles Programme (P7/05) initiated by the Belgian Science Policy Office. The authors would also like to thank Prof. Denis Jacquemin for the helpful suggestions and Andy Van Yperen – De Deyne, Lien Van der Schueren and Lennart Joos for fruitful discussions.

Appendix A. Supplementary data

Supplementary data related to this article can be found at http://dx.doi.org/10.1016/j.dyepig.2013.10.048.

References

[1] Zollinger H. Color chemistry: synthesis, properties, and applications of organic dyes and pigments. VHCA en WILEY-VCH; 2003.
[2] Kim S. Functional dyes. Elsevier; 2006.
[3] Bamfield P. Chromic phenomena, technological applications of colour chemistry. Royal Society of Chemistry; 2001.
[4] Little AF, Christie RM. Textile applications of photochromic dyes. Part 1: establishment of a methodology for evaluation of photochromic textiles using traditional colour measurement instrumentation. Color Technol 2010;126:157–63.
[5] Rubacha M. Thermochromic cellulose fibers. Polym Adv Technol 2007;18:323–8.
[6] De Meyer T, Hemelsoet K, Van Der Schueren L, Pauwels E, De Clerck K, Van Speybroeck V. Investigating the halochromic properties of azo dyes in an aqueous environment by using a combined experimental and theoretical approach. Chem Eur J 2012;18:8120–9.
[7] Roy D, Cambre JN, Sumerlin BS. Future perspectives and recent advances in stimuli-responsive materials. Prog Polym Sci 2010;35:278–301.
[8] Emond M, Sun J, Gregoire J, Maurin S, Tribet C, Jullien L. Photoinduced pH drops in water. Phys Chem Chem Phys 2011;13:6493–9.
[9] Mohr GJ, Wolfbeis OS. Optical sensors for a wide pH range based on azo dyes immobilized on a novel support. Anal Chim Acta 1994;292:41–8.
[10] Kuwabara T, Nakajima H, Nanasawa M, Ueno A. Color change indicators for molecules using methyl red modified cyclodextrins. Anal Chem 1999;71:2844–9.
[11] Van der Schueren L, De Clerck K. The use of pH-indicator dyes for pH-sensitive textile materials. Text Res J 2009;80:590–603.
[12] Trupp S, Alberti M, Carofiglio T, Lubian E, Lehmann H, Heuermann R, et al. Development of pH-sensitive indicator dyes for the preparation of micropatterned optical sensor layers. Sens Actuators B 2010;150:206–10.
[13] Kirschning A, Monenschein H, Wittenberg R. Functionalized polymers-emerging versatile tools for solution-phase chemistry and automated parallel synthesis. Angew Chem Int Ed 2001;40:650–79.
[14] Vancoillie G, Pelz S, Holder E, Hoogenboom R. Direct nitroxide mediated (co) polymerization of 4-vinylphenylboronic acid as route towards sugar sensors. J Polym Sci A Polym Chem 2012;3:1726–9.
[15] Pietsch C, Schubert U, Hoogenboom R. Aqueous polymeric sensors based on temperature-induced polymer phase transitions and solvatochromic dyes. Chem Commun 2011;47:8750–65.
[16] Fournier D, Prez FD. Click chemistry as a promising tool for side-chain functionalization of polyurethanes. Macromolecules 2008;41:4622–30.
[17] Van der Schueren L, Mollet T, Ceylan O, De Clerck K. The development of polyamide 6.6 nanofibres with a pH-sensitive function by electrospinning. Eur Polym J 2010;46:2229–39.
[18] Van der Schueren L, De Clerck K. Textile materials with a pH-sensitive function. Int J Cloth Sci Tech 2011;23:269–74.
[19] Van der Schueren L, De Clerck K. Coloration and application of pH-sensitive dyes on textile materials. Color Technol 2012;128:82–90.
[20] Van der Schueren L, Hemelsoet K, Van Speybroeck V, De Clerck K. The influence of a polyamide matrix on the halochromic behaviour of the pH-sensitive azo dye nitrazine yellow. Dyes Pigm 2012;94:443–51.
[21] Van Der Schueren L, De Meyer T, Steyaert I, Ceylan O, Hemelsoet K, Van Speybroeck V, et al. Polycaprolactone and polycaprolactone/chitosan nanofibres functionalised with the pH-sensitive dye nitrazine yellow. Carbohydr Polym 2013;91:284–93.
[22] Staneva D, Betcheva R, Chovelon JM. Optical sensor for aliphatic amines based on the simultaneous colorimetric and fluorescence responses of smart textile. J Appl Polym Sci 2007;106:1950–6.
[23] Li G, Xiao J, Zhang W. A novel dual colorimetric fiber based on two acidbase indicators. Dyes Pigm 2012;92:1091–9.
[24] Egawa Y, Hayashida R, Anzai J. Multilayered assemblies composed of brilliant yellow and poly(allylamine) for an optical pH sensor. Anal Sci 2006;22:1117–9.
[25] Wang H, Callahan PM. Adsorption studies of azo dyes as resonance Raman spectroscopic probes at solid-liquid interfaces. J Chromatogr A 1998;828:121–34.
[26] Canamares MV, Garcia-Ramos JV, Domingo C, Sanchez-Cortes S. Surface-enhanced Raman scattering study of the adsorption of the anthraquinone pigment alizarin on Ag nanoparticles. J Raman Spectrosc 2004;35:921–7.
[27] Fabbri P, Pilati F, Rovati L, McKenzie R, Mijovic J. Poly(ethylene oxide)-silica hybrids entrapping sensitive dyes for biomedical optical pH sensors: molecular dynamics and optical response. Opt Mat 2011;33:1362–9.
[28] Capel-Cuevas S, Cuellar MP, de Orbe-Paya I, Pegalajar MC, Capitan-Vallvey LF. Full-range optical pH sensor based on imaging techniques. Anal Chim Acta 2010;681:71–81.
[29] Tao X, Li J, Möhwald H. Self-assembly, optical behavior, and permeability of a novel capsule based on an azo dye and polyelectrolytes. Chem Eur J 2004;10:3397–403.
[30] Staneva D, Betcheva R, Chovelon JM. Fluorescent benzo de anthracen-7-one pH-sensor in aqueous solution and immobilized on viscose fabrics. J Photochem Photobiol A 2006;183:159–64.
[31] Ertekin K, Cinar S, Aydemir T, Alp S. Glucose sensing employing fluorescent pH indicator: 4-[(-,-dimethylamino)benzylidene]-2-phenyloxazole-5-one. Dyes Pigm 2005;67:133–8.
[32] Machida K, Lee H, Uno T. Resonance Raman spectra of sulfophthalein dyes in aqueous solutions. J Raman Spectrosc 1979;8:172–6.
[33] Christie RM, Morgan KM, Islam MS. Molecular design and synthesis of N-arylsulfonated coumarin fluorescent dyes and their application to textiles. Dyes Pigm 2008;76:741–7.
[34] Waring DR, Hallas G. Topics in applied chemistry: the chemistry and application of dyes. Plenum Press; 1990.
[35] Macka M, Andersson P, Haddad PR. Changes in electrolyte pH due to electrolysis during capillary zone electrophoresis. Anal Chem 1998;70:743–9.
[36] Fujii T, Toriumi K. Ultravioletvisible absorption spectra of thymol blue during the solgelxerogel transition of tetraethyl orthosilicate: in situ probe of microchemical environment. J Chem Soc Faraday Trans 1 1993;89:3437–41.
[37] Flores R. A rapid and reproducible assay for quantitative estimation of proteins using bromophenol blue. Anal Biochem 1978;88:605–11.
[38] You L, Wu Z, Kim T, Lee K. Kinetics and thermodynamics of bromophenol blue adsorption by a mesoporous hybrid gel derived from tetraethoxysilane and bis (trimethoxysilyl) hexane. J Colloid Interface Sci 2006;300:526–35.
[39] Ghaedi M, Khajesharifi H. Cadmium hydroxide nanowire loaded on activated carbon as efficient adsorbent for removal of bromocresol green. Spectrochim Acta A 2012;86:62–8.
[40] Drummond C, Grieser F, Healy T. Acidbase equilibria in aqueous micellar solutions. Part 2. Sulphonephthalein indicators. J Chem Soc Faraday Trans 1 1989;85:537–50.
[41] Buvári A, Barcza L, Kajtár M. Complex formation of phenolphthalein and some related compounds with β-cyclodextrin. J Chem Soc Perkin Trans 2 1988:1687–90.
[42] Burford G, Pickering B. The number of neurophysins in the rat. Influence of the concentration of bromophenol blue, used as a tracking dye, on the resolution of proteins by polyacrylamide-gel. Biochem J 1972;128:941.
[43] Kurzweilová H, Sigler K. Fluorescent staining with bromocresol purple: a rapid method for determining yeast cell dead count developed as an assay of killer toxin activity. Yeast 1993;9:1207–11.
[44] Webster D. A study of the interaction of bromocresol green with isolated serum globulin fractions. Clin Chim Acta 1974;53:109–15.
[45] Marona H, Schapoval E. Spectrophotometric determination of sparfloxacin in pharmaceutical formulations using bromothymol blue. J Pharm Biomed Anal 2001;26:501–4.
[46] Robertson J. Bromothymol blue broth: improved medium for detection of ureaplasma urealyticum (T-strain mycoplasma). J Clin Microbiol 1978;7:127–32.
[47] Baylor SM, Hollingworth S. Absorbency signals from resting frog skeletal-muscle fibers injected with the pH indicator dye, phenol red. J Gen Physiol 1990;96:449–71.
[48] Berthois Y, Katzenellenbogen JA, Katzenellenbogen BS. Phenol red in tissue-culture media is a weak estrogen – implications concerning the study of estrogen-responsive cells in culture. Proc Natl Acad Sci U S A 1986;83:2496–500.
[49] Byrne RH, Breland JA. High-precision multiwavelength pH determinations in seawater using cresol red. Deep-Sea Res Oceanogr A 1989;36:803–10.
[50] Bellerby RGJ, Olsen A, Johannessen T, Croot P. A high precision spectrophotometric method for on-line shipboard seawater pH measurements: the automated marine pH sensor (AMpS). Talanta 2002;56:61–9.
[51] Clayton TD, Byrne RH. Spectrophotometric seawater pH measurements: total hydrogen results. Deep-Sea Res Oceanogr A 1993;40:2115–29.
[52] Zhang H, Byrne RRH. Spectrophotometric pH measurements of surface seawater at in-situ conditions: absorbance and protonation behavior of thymol blue. Mar Chem 1996;52:17–25.
[53] Yao W, Byrne R. Spectrophotometric determination of freshwater pH using bromocresol purple and phenol red. Environ Sci Technol 2001;35:1197–201.
[54] Andres R, Narayanaswamy R. Fibre-optic pesticide biosensor based on covalently immobilized acetylcholinesterase and thymol blue. Talanta 1997;44:1335–52.

[55] Nakamura N, Amao Y. An optical sensor for CO_2 using thymol blue and europium (III) complex composite film. Sens Actuators B 2003;92:98–101.
[56] Chang Y, Bai H, Li S, Kuo C. Bromocresol green/mesoporous silica adsorbent for ammonia gas sensing via an optical sensing instrument. Sensors 2011;11:4060–72.
[57] Ensafi A. Poly(xylenol blue) modified multiwall carbon nanotubes-glassy carbon electrode for simultaneous determination of ascorbic acid, epinephrine, and uric acid by differential. In: Enabling science and nanotechnology, Kuala Lumpur 2010.
[58] Yang G, Yan J, Qi F, Sun C. Poly (bromocresol purple) film modified glassy carbon electrode for determination of trace amount of cadmium by differential pulse anodic stripping voltammetry. Electroanalysis 2010;22:2729–38.
[59] Hua X, Hou X, Gong X, Shen G. Electrochemical behaviour of 5-fluorouracil on glassy carbon electrode modified with bromothymol blue and multi-walled carbon nanotubes. Anal Methods 2013;5:2470–6.
[60] Chen W, Lin XH, Huang LY, Luo HB. Electrochemical characterization of polymerized cresol red film modified glassy carbon electrode and separation of electrocatalytic responses for ascorbic acid and dopamine oxidation. Microchim Acta 2005;151:101–7.
[61] Ray P, Das P. First-order hyperpolarizabilities of sulfophthalein dyes. J Phys Chem 1995;99:14414–7.
[62] Bhuchar VM, Agrawal AK. Evaluation of colour changes of sulphamphthalein indicators: synthesis, purification and characterisation of phenol- and o-cresolsulphamphthalein. Analyst 1982;107:1439–50.
[63] Runge E, Gross E. Density-functional theory for time-dependent systems. Phys Rev Lett 1984;52:997–1000.
[64] Petersilka M, Gossmann U, Gross E. Excitation energies from time-dependent density-functional theory. Phys Rev Lett 1996;76:1212–5.
[65] Marques MAL, Gross EKU. Time-dependent density functional theory. Annu Rev Phys Chem 2004;55:427–55.
[66] Adamo C, Jacquemin D. The calculations of excited-state properties with time-dependent density functional theory. Chem Soc Rev 2013;42:845–56.
[67] Tozer D, Handy N. On the determination of excitation energies using density functional theory. Phys Chem Chem Phys 2000;2:2117–21.
[68] Dreuw A, Head-Gordon M. Failure of time-dependent density functional theory for long-range charge-transfer excited states: the zincbacteriochlorin-bacteriochlorin and bacteriochlorophyll-spheroidene. J Am Chem Soc 2004;126:4007–16.
[69] Iikura H, Tsuneda T, Yanai T, Hirao K. A long-range correction scheme for generalized-gradient-approximation exchange functionals. J Chem Phys 2001;115:3540–4.
[70] Tawada Y, Tsuneda T, Yanagisawa S, Yanai T, Hirao K. A long-range-corrected time-dependent density functional theory. J Chem Phys 2004;120:8425–33.
[71] Yanai T, Tew DP, Handy NC. A new hybrid exchangecorrelation functional using the Coulomb-attenuating method (CAM-B3LYP). Chem Phys Lett 2004;393:51–7.
[72] Abbott LC, Batchelor SN, Oakes J, Gilbert BC, Whitwood AC, Smith JRL, et al. Experimental and computational studies of structure and bonding in parent and reduced forms of the azo dye orange II. J Phys Chem A 2005;109:2894–905.
[73] Teimouri A, Chermahini AN, Emami M. Synthesis, characterization, and DFT studies of a novel azo dye derived from racemic or optically active binaphthol. Tetrahedron 2008;64:11776–82.
[74] Teimouri A, Chermahini AN, Taban K, Dabbagh HA. Experimental and CIS, TD-DFT, ab initio calculations of visible spectra and the vibrational frequencies of sulfonyl azide-azoic dyes. Spectrochim Acta A 2009;72:369–77.
[75] Snehalatha M, Ravikumar C, Joe IH. Spectroscopic investigations and ab initio computations of the dye chromotrope 2R. Solid State Sci 2009;11:1275–82.
[76] Walkup LL, Weerasinghe KC, Tao ML, Zhou XQ, Zhang MH, Liu DZ, et al. Importance of dynamics in electron excitation and transfer of organic dyes. J Phys Chem C 2010;114:19521–8.
[77] Guillaumont D, Nakamura S. Calculation of the absorption wavelength of dyes using time-dependent density-functional theory (TD-DFT). Dyes Pigm 2000;46:85–92.
[78] Briquet L, Vercauteren DP, André J-M, Perpète EA, Jacquemin D. On the geometries and UV/Vis spectra of substituted trans-azobenzenes. Chem Phys Lett 2007;435:257–62.
[79] Jacquemin D, Perpete EA, Scuseria GE, Ciofini I, Adamo C. TD-DFT performance for the visible absorption spectra of organic dyes: conventional versus long-range hybrids. J Chem Theory Comput 2007;4:123–35.
[80] Jacquemin D, Perpete EA, Ciofini I, Adamo C. On the TD-DFT UV/vis spectra accuracy: the azoalkanes. Theor Chem Acc 2008;120:405–10.
[81] Jacquemin D, Wathelet V, Perpete A, Adamo C. Extensive TD-DFT benchmark: singlet-excited states of organic molecules. J Chem Theory Comput 2009;5:2420–35.
[82] Jacquemin D, Preat J. Absorption spectra of azobenzenes simulated with time-dependent density functional theory. Int J Quantum Chem 2011;111:4224–40.
[83] Jacquemin D, Perpete EA, Ciofini I, Adamo C, Valero R, Zhao Y, et al. On the performances of the M06 family of density functionals for electronic excitation energies. J Chem Theory Comput 2010;6:2071–85.
[84] Charaf-Eddin A, Planchat A, Mennucci B, Adamo C, Jacquemin D. Choosing a functional for computing absorption and fluorescence band shapes with TD-DFT. J Chem Theory Comput 2013;9:2749–60.
[85] Peach MJG, Benfield P, Helgaker T, Tozer DJ. Excitation energies in density functional theory: an evaluation and a diagnostic test. J Chem Phys 2008;128:044118.
[86] Peach M, Sueur CL. TDDFT diagnostic testing and functional assessment for triazene chromophores. Phys Chem Chem Phys 2009;11:4465–70.
[87] Peach M, Tozer D. Illustration of a TDDFT spatial overlap diagnostic by basis function exponent scaling. J Mol Struct Theochem 2009;914:110–4.
[88] Sears J, Koerzdoerfer T, Zang C-R, Bredas J-L. Orbital instabilities and triplet states from time-dependent density functional theory and long-range corrected functionals. J Chem Phys 2011;135:151103–6.
[89] Peach MJG, Williamson MJ, Tozer DJ. Influence of triplet instabilities in TDDFT. J Chem Theory Comput 2011;7:3578–85.
[90] Peach MJG, Tozer DJ. Overcoming low orbital overlap and triplet instability problems in TDDFT. J Phys Chem A 2012;116:9783–9.
[91] Van der Schueren L, De Clerck K, Brancatelli G, Rosace G, Van Damme E, De Vos W. Novel cellulose and polyamide halochromic textile sensors based on the encapsulation of methyl red into a solgel matrix. Sens Actuators B 2012;162:27–34.
[92] Wojciechowski K. Halochromic effects of azophthalimide dyes and their prediction by PPP method. Dyes Pigm 1996;32:199–208.
[93] Frisch MJ, Trucks GW, Schlegel HB, Scuseria GE, Robb MA, Cheeseman JR, et al. Gaussian09 RevB. Wallingford CT: Gaussian Inc.; 2009.
[94] Becke AD. Density functional thermochemistry. III. The role of exact exchange 98:5648-52. J Chem Phys 1993;103:361–3.
[95] Chengteh L, Weitao Y, Parr RG. Development of the Colle-Salvetti correlation-energy formula into a functional of the electron density. Phys Rev B Condens Matter 1988;37:785–9.
[96] Özen AS, Aviyente V, De Proft F, Geerlings P. Modeling the substituent effect on the oxidative degradation of azo dyes. J Phys Chem A 2004;108:5990–6000.
[97] Ozen AS, Doruker P, Aviyente V. Effect of cooperative hydrogen bonding in azo-hydrazone tautomerism of azo dyes. J Phys Chem A 2007;111:13506–14.
[98] Ucun F, Salam A, Kara I, Karci F, Saglam A, Karci F. Investigation of ground state tautomeric form of a heterocyclic disazo dye derived from barbituric acid by ab initio Hartree-Fock and density functional theory calculations. J Mol Struct Theochem 2008;868:94–100.
[99] Kunov-Kruse AJ, Kristensen SB, Liu C, Berg RW. Experimental and ab initio DFT calculated Raman spectrum of Sudan I, a red dye. J Raman Spectrosc 2010;42:1470–8.
[100] Curtiss L, Raghavachari K. Investigation of the use of B3LYP zero-point energies and geometries in the calculation of enthalpies of formation. Chem Phys Lett 1997;2614.
[101] Moller C, Plesset MS. Note on approximation treatment for many-electron systems. Phys Rev 1934;46:618.
[102] Ho JM, Klamt A, Coote ML. Comment on the correct use of continuum solvent models. J Phys Chem A 2010;114:13442–4.
[103] Perdew JP, Burke K, Ernzerhof M. Generalized gradient approximation made simple. Phys Rev Lett 1996;77:3865–8.
[104] Perdew JP, Burke K, Ernzerhof M. Errata: generalized gradient approximation made simple. Phys Rev Lett 1997;78:1396.
[105] Zhao Y, Truhlar DG. The M06 suite of density functionals for main group thermochemistry, thermochemical kinetics, noncovalent interactions, excited states, and transition elements: two new functionals and systematic testing of four M06-class functionals and 12 other function. Theor Chem Acc 2008;120:215–41.
[106] Orozco M, Luque FJ. Theoretical methods for the description of the solvent effect in biomolecular systems. Chem Rev 2000;100:4187–226.
[107] Tomasi J, Persico M. Molecular-interactions in solution – an overview of methods based on continuous distributions of the solvent. Chem Rev 1994;94:2027–94.
[108] Tomasi J, Mennucci B, Cammi R. Quantum mechanical continuum solvation models. Chem Rev 2005;105:2999–3094.
[109] Lund H, CCXXXIX. The constitution of phenolphthalein. Part II. The fading of phenolphthalein in alkaline solution. J Chem Soc (Res) 1930:1844–52.
[110] Kolthoff I, Rosenblum C. Acid-base indicators. New York: Macmillan; 1937.
[111] Furche F, Ahlrichs R. Adiabatic time-dependent density functional methods for excited state properties. J Chem Phys 2002;117:7433–47.
[112] Schreiber M, Buß V, Fülscher M. The electronic spectra of symmetric cyanine dyes: a CASPT2 study. Phys Chem Chem Phys 2001;3.
[113] Meguellati K, Ladame S, Spichty M. A conceptually improved TD-DFT approach for predicting the maximum absorption wavelength of cyanine dyes. Dyes Pigm 2011;90:114–8.
[114] Send R, Valsson O, Filippi C. Electronic excitations of simple cyanine dyes: reconciling density functional and wave function methods. J Chem Theory Comput 2011;7:444–55.
[115] Jacquemin D, Zhao Y, Valero R, Adamo C, Ciofini I, Truhlar DG. Verdict: time-dependent density functional theory not guilty of large errors for cyanines. J Chem Theory Comput 2012;8:1255–9.
[116] Jacquemin D, Planchat A, Adamo C, Mennucci B. TD-DFT assessment of functionals for optical 00 transitions in solvated dyes. J Chem Theory Comput 2012;8:2359–72.

[117] Toth AM, Liptak MD, Phillips DL, Shields GC. Accurate relative pK_a calculations for carboxylic acids using complete basis set and Gaussian-n models combined with continuum solvation methods. J Chem Phys 2001;114:4595.
[118] Mohr GJ, Müller H, Bussemer B, Heuermann R, Henkel T, Escudero D, et al. Design of acidochromic dyes for facile preparation of pH sensor layers. Anal Bioanal Chem 2008;392:1411–8.
[119] Namazian M, Zakery M, Noorbala MR, Coote ML. Accurate calculation of the pKa of trifluoroacetic acid using high-level ab initio calculations. Chem Phys Lett 2008;451:163–8.
[120] Ho J, Coote M. pKa calculation of some biologically important carbon acids – an assessment of contemporary theoretical procedures. J Chem Theory Comput 2009;5:295–306.
[121] Ho J, Coote ML. First-principles prediction of acidities in the gas and solution phase. Wiley Interdiscip Rev Comput Mol Sci 2011;1:649–60.
[122] Liptak MD, Shields GC. Accurate pKa calculations for carboxylic acids using complete basis set and Gaussian-n models combined with CPCM continuum solvation methods. J Am Chem Soc 2001;123:7314–9.
[123] Schmidt M, Knapp E-W. Accurate pKa determination for a heterogeneous group of organic molecules. Chem Phys Phys Chem 2004;5:1513–22.